Fast ion confinement in the three-dimensional helical reversed-field pinch

Fast ion confinement in the three-dimensional helical reversed-field pinch

J K Anderson[1]**, W Capecchi**[1]**, S Eilerman**[1]**, J J Koliner**[1]**, M D Nornberg**[1]**,
J A Reusch**[1]**, J S Sarff**[1] **and L Lin**[2]

[1] University of Wisconsin, Department of Physics, Madison WI, USA
[2] University of California- Los Angeles, Department of Physics, Los Angeles CA, USA

E-mail: jkanders@wisc.edu

Abstract

Fast ions are well confined in the stochastic magnetic field of the multiple-helicity (MH) reversed-field pinch (RFP), with fast ion confinement times routinely a factor of 5 to 10 higher than thermal confinement time. Recent experiments have examined the behavior and confinement of beam-born fast ions in the three-dimensional (3D) helical RFP state. In lower current discharges, where the onset of the helical state is uncertain, high power neutral beam injection (NBI) tends to suppress the transition to the single helicity mode. In high current discharges ($I_p \sim 0.5\,\text{MA}$), where the onset of $n = 5$ single helicity is quite robust, a short blip of NBI is used to probe the confinement of fast ions with minimal perturbation to the 3D equilibrium. The fast ion confinement time is measured to be substantially lower than fast ions in comparable MH RFP states, and there is a strong dependence on the strength of the helical perturbation. The established helical equilibrium is stationary in the laboratory frame but the locking occurs over the entire range of possible phase with respect to the Madison Symmetric Torus vessel. This effectively scans both the location of the NBI with respect to the helical structure and the pitch of the NBI-born fast ions. Fast ion confinement is observed to be insensitive to this angle, and in fact counter-NB injection into quasi-single helicity discharges shows fast ion confinement times similar to co-injection cases, in contrast to the MH RFP, where counter-injected fast ion confinement time is substantially lower.

Keywords: fast ion confinement, RFP, quasi-single helicity

(Some figures may appear in colour only in the online journal)

1. Introduction

The confinement of fast ions is critical for any magnetic fusion concept as plasma self-heating is essential for a burning plasma. While well studied in the tokamak [1], stellarator [2] and ST [3], the confinement of fast ions in the reversed-field pinch (RFP) configuration is still in its initial exploration. Fast ions are observed to be very well confined in the stochastic magnetic field of the RFP [4, 5] by comparison of the d–d fusion rate following a blip of neutral beam injection (NBI). The measured fusion neutron flux decay approaches that expected from classical slowing alone, and implies fast particle confinement times more than an order of magnitude above thermal particle confinement time. This remarkable result is due to the fast ion's insensitivity to multiple tearing modes' magnetic fluctuations that govern thermal transport.

A second fascinating observation of the RFP plasma is a spontaneous self-organization to a three-dimensional (3D) state dominated by a single helical perturbation [6, 7] referred to in this work as quasi-single helicity (QSH). The transition tends to occur in plasmas with lower resistive dissipation, found in higher plasma current, lower density discharges [8]. This transition and consequential helical equilibrium has received a good deal of attention, and in particular has spurred collaboration between physicists in the stellarator and RFP communities. As the likelihood of this state increases

with plasma current, it could be expected to be an important consideration of the envisioned next step, higher current RFPs.

In this work, we document a pair of new observations from neutral beam injection into QSH RFP discharges. In section 2, we discuss the first measurement of fast ion confinement in the 3D, helical RFP. A beam blip technique [9] is again employed, keeping the number of fast ions small and non-perturbative. The fast ions do not approach the classical confinement limit in this case; there is a factor of about 20 reduction in fast ion confinement time from the multiple helicity (MH) to QSH state.
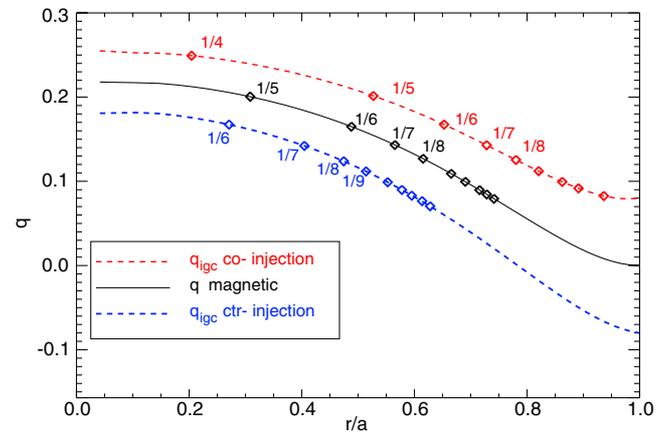
In section 3, we consider the effect of a large fast ion population in the discharges conducive to transition to a QSH state. While there is a solid empirical understanding of the proper conditions to trigger a QSH transition, the detailed physics are not understood [10]. High power neutral beam injection tends to suppress the transition to QSH in marginal target discharges; this is likely related to a prior observation of core-most tearing amplitude being suppressed by NBI in the RFP [11].

2. Fast ion confinement in 3D RFP state

Routine operation of Madison Symmetric Torus (MST) [12] includes plasma current up to $500\,\text{kA}$, with a range of line-averaged electron density of 0.5–$2.0 \times 10^{13}\,\text{cm}^{-3}$. The toroidal magnetic field at the wall is a boundary condition which can be finely controlled to enable operation with $q(a)$ between $-.15$ and zero. In figure 1, a representative q profile is shown for a $q(a) = 0$ discharge (solid line), and illustrates the spectra of dominant resonant tearing modes, which govern much of the macroscopic plasma dynamics [13]. Magnetic islands of finite width (set by strength of the local radial magnetic field perturbation) can overlap and cause field lines (and magnetized particle orbits) to become stochastic. Discharges with substantially reversed $q(a)$ often exclude the $q = 1/5$ resonance which exists as the core-most mode in this example.

Fast ions (in low concentration) are observed to be much better confined than thermal particles in the standard RFP as the finite guiding center drifts move the fast ions to a different rotational transform. This affects the fast ion interaction with magnetic fluctuations [14]. The effective fast ion safety factor, $q_{\text{fi}} = \frac{\omega_\phi}{\omega_\theta} = \frac{r v_\phi}{R v_\theta}$, is the ratio of the fast ion toroidal and poloidal guiding center orbit frequencies and is analogous to the magnetic q (q_{MHD}) profile for identification of resonances. Plotted in dashed lines in figure 1 are q_{fi} for co- (red) and counter- (blue) injected $25\,\text{kV}$ NBI ions (pitch = .8). The analogous fast ion guiding center islands, and island widths, are set by the radial velocity perturbation at the rational surface in the q_{fi} profile. This is related to the magnetic perturbation of the same helicity, but as the radius of resonant interaction is removed from the magnetic resonance, the magnetic fluctuation strength is lower.

In particular, for co-injected fast ions q_{fi} is shifted upward from q_{MHD}, leading to an outward shift of the resonant surfaces identified in the q_{MHD} profile. This also makes the core-most $m = 1$ fast ion rational surface correspond to $n = 4$—a helicity without a corresponding resonant magnetic perturbation within the plasma. There is also a substantial radial domain in the core
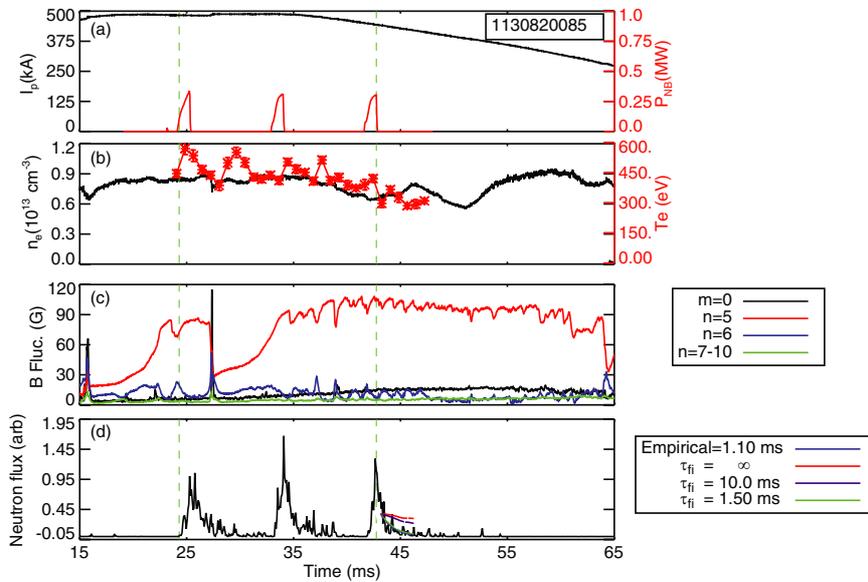

Figure 1. An example safety factor profile with $q(a) = 0$ in an axisymmetric MST discharge is plotted in black, with locations of rational surfaces where tearing modes with $m = 1$ and varying n resonantly exist. The $q(a) = 0$ boundary condition is achieved by applying zero toroidal magnetic field current. In this case $q(0) > 1/5$, making the $m = 1$, $n = 5$ mode the core-most resonant tearing mode. Also plotted are the effective fast ion guiding center q profiles, $q_{\text{fi}} = r v_\phi / R v_\theta$ for co- and counter-injected $25\,\text{kV}$ fast ions which illustrate a substantial deviation from magnetized particles due to the large drift.

free of ion guiding center resonances. These features make core-localized fast ions insensitive to the stochastic magnetic transport, rendering them nearly classically confined. As the fast ions slow, $\Delta q = q_{\text{fi}} - q_{\text{MHD}}$ decreases; eventually the fast ion resonances overlap with magnetic resonances causing the particle orbits to become radially stochastic.

The counter injection case has a reduced q_{fi} with respect to q_{MHD}. This leads to more closely spaced rational surfaces, all of which have resonant magnetic perturbations within the plasma. As the relevant helicity magnetic perturbation at the fast ion rational surface is reduced from its maximum value (found at higher radius at the resonant surface in q_{MHD} [15]), the counter-injected fast ions are still better confined than thermal particles, however there is no region in which radially unperturbed fast ion orbits are expected.

Fast ion confinement phenomenology is different in the QSH RFP. The transition to QSH occurs most robustly at high Lundquist number, achieved in practice by high plasma current and low electron density, resulting in maximum magnetic field strength and lowest plasma resistivity. Additionally, the transition to QSH occurs with a low degree of toroidal field reversal. It is most commonly observed in MST with zero field reversal, $q(a) = 0$, as illustrated in figure 1. The aspect ratio of MST dictates that the $n = 5$ toroidal mode is the core-most resonant $m = 1$ mode in these cases, and the observed QSH state in MST is distinctly $n = 5$ in character.

In figure 2, a typical discharge and experimental technique for measuring fast ion confinement are illustrated. figure 2(a) shows the plasma current of about $500\,\text{kA}$, near the MST maximum, and three short blips of $25\,\text{kV}$ deuterium NBI. This keeps the total fast ion content low to avoid perturbations to the equilibrium or destabilizing energetic particle driven modes. Figure 2(b) shows the necessary time resolved kinetic measurements of line integrated electron density (interferometry) and core electron temperature
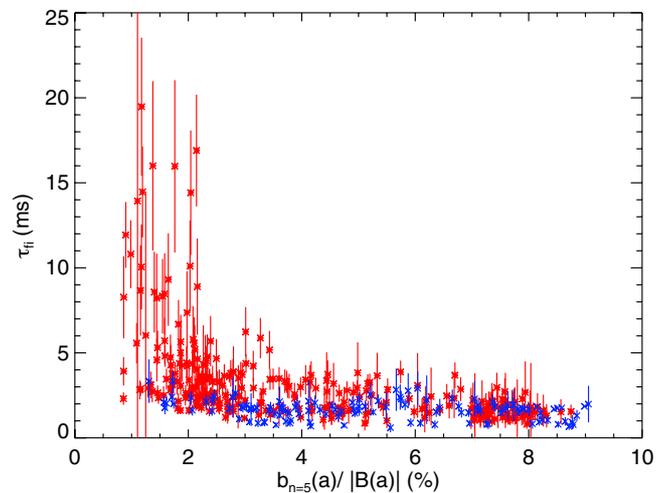
Figure 2. Typical discharge where fast ion confinement is measured in the RFP QSH state. Plots versus time are shown of: (*a*) plasma current and NBI power; (*b*) line-averaged electron density and core electron temperature; (*c*) edge-measured magnetic activity, which identifies transitions to/from QSH state; (*d*) beam–target neutron flux, from which fast ion confinement is inferred.

(Thomson scattering) for computing the classical slowing of the NBI-born fast ions.

In figure 2(*c*), the edge-measured magnetic mode amplitudes reveal the signatures of transition to (and relaxation out of) the QSH mode. In this example, there are two transitions into QSH, that occur when the amplitude of the $n = 5$ mode (red line) grows rapidly and secondary modes (represented by the $n = 6$ (blue line) and $n = 7$–10 combined (green line) amplitudes) decrease. At $t = 27$ ms, a large burst of $m = 0$ (black line) magnetic activity coincides with a relaxation back to the MH state. Figure 2(*d*) is a plot of the d–d fusion neutron flux measured by a lead-shielded scintillator and PMT, with three distinct increases due to NBI. Each time the NBI is switched off, the source of fast ions is removed and the neutron flux decays exponentially. The bulk plasma d–d fusion rate in these discharges is below the resolution of the diagnostic. The measured decay of neutron flux τ_n is compared with that expected from classical slowing alone τ_{cl}; any deviation (faster decay) indicates a finite confinement time of the fast ions according to $1/\tau_n = 1/\tau_{cl} + 1/\tau_{fi}$. The curves on the third beam blip in figure 2(*d*) are an example of the fast ion confinement time fitting: the red line is the expected fusion neutron flux decay rate for classical slowing alone; the best fit to the data for this example corresponds to a fast ion confinement time of $\tau_{fi} = 1.1$ ms.
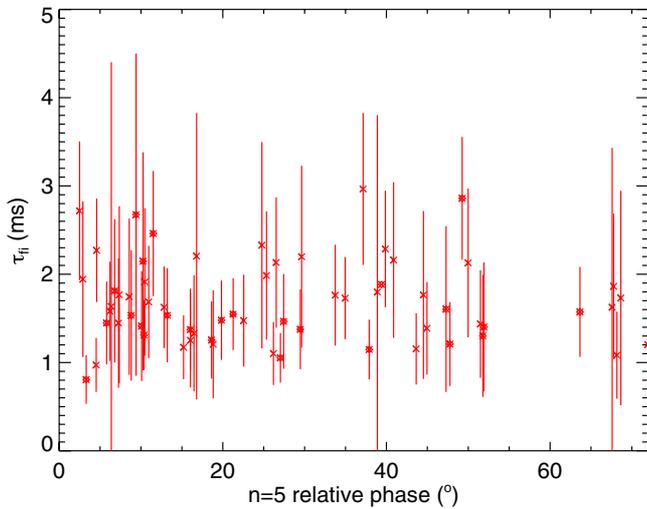
While figure 2(*c*) plots the edge-measured amplitude (in Gauss), a more appropriate measure of the strength of the $n = 5$ helical perturbation is the ratio of the edge-measured amplitude to the edge magnetic field strength (proportional to the plasma current). With this metric, it is possible to compare between discharges with slightly different plasma current, and to include time points in the initial stages of the current ramp down that marks the end of the discharge (note I_p is decreasing at the time of third blip in figure 2(*a*)).

The beam is programmed to blip at particular times in the discharge, far enough apart to allow beam–target fusion

Figure 3. Measured fast ion confinement time versus edge-measured amplitude of $n = 5$ mode (an indicator of the QSH state). Plotted in red are co-injected fast ions, in blue are counter-injected fast ions. Recall that as the $n = 5$ mode becomes small, secondary mode amplitudes are larger and magnetic stochasticity is generally enhanced. In the limit of low $n = 5$ amplitude the fast ion confinement rapidly grows to near classical levels for co-injected ions. Counter-injected fast ions have a much lower confinement time in the stochastic RFP. In the QSH state, note the similarity between co- and counter-injected fast ions at a given mode amplitude.

neutrons to vanish before the next pulse, and is repeated over many discharges. The discharges have slightly different plasma current (between 460 and 510 kA at the beam blip), and slightly varied $q(a)$ (between $-.008$ and 0). By changing these plasma parameters, the normalized strength of the helical perturbation is swept over a wide range. The measured fast ion confinement time versus normalized field strength is plotted in figure 3. The points in red represent injection of fast ions tangentially in the direction of plasma current, while those in blue are counter injected fast ions.
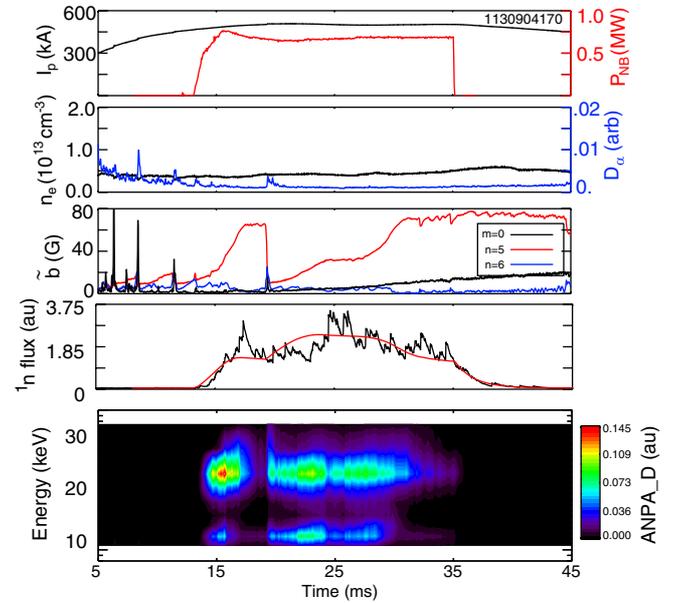
Figure 4. Measured fast ion confinement time (co-injected fast ions) versus phase of $n = 5$ mode at a particular $n = 5$ amplitude of 7.5% of $|B(a)|$. As the structure locks in the laboratory frame at random angles, this is an effective scan of the tangential NBI location with respect to the helical plasma equilibrium and initial pitch angle distribution of fast ions. Fast ion confinement is not sensitive to pitch in the QSH state.

There are several observations to draw from the data. Consider first the co-injected ions. At low values of $n = 5$ helical perturbation, around 1% or less, the measured fast ion confinement time rapidly increases toward classical values as previously reported [4, 5]. However, as the helical perturbation becomes significant, the fast ion confinement time falls roughly obeying a $\tau_{fi} \propto 1/\tilde{b}$ dependence. Although there is a large uncertainty in each measured point and considerable scatter in the data, it is clear that a change occurs with the growth of a helical perturbation.

The stark difference between co-injected and counter-injected fast ions in the stochastic field disappears in the QSH state. There is no distinguishable co- versus counter-difference in the measured fast ion confinement time in the well-established QSH state ($\tilde{b}_{n=5}/|B(a)| > 5\%$).

During (or sometimes before) the transition to QSH, the $n = 5$ deformation locks in the laboratory frame with a random phase. The range of locking phases covers all angles with respect to the MST vessel and NBI. This effectively scans the location of the NBI and the core-localized initial pitch of the injected fast ions. A subset of the co-injected data from figure 3 with $7\% < \tilde{b}_{n=5}/|B(a)| < 8\%$ is re-examined as a function of the helical mode phase angle and plotted in figure 4. There is no noticeable effect of the $n = 5$ phase (initial fast ion pitch) on the fast ion confinement time. This observation reinforces the co-/counter-injected fast ion time equality (figure 3) and implies no τ_{fi} dependence on pitch.

In figure 5, we consider a second example of NBI into a discharge conducive to transitioning to QSH. In this case, a 20 ms pulse of deuterium NBI (at nearly 0.8 MW injected) starts as the $n = 5$ mode begins to grow (indicative of transition into QSH). Figure 5(*a*) is the plasma current and NB power, 5(*b*) is the electron density and D_α emission (a signal related to neutral density within the plasma), and 5(*c*) shows the magnetic

Figure 5. Example of full 20 ms pulse of deuterium NBI into a discharge conducive to QSH transition. In (*a*), the plasma current and neutral beam power; (*b*) the electron density and D_α emission; (*c*) the $n = 5$, $n = 6$ and $m = 0$ magnetic activity; (*d*) the measured and simple model predicted d–d fusion neutron flux; and (*e*) the energy distribution of core-localized, high pitch ions are plotted.

activity of the dominant $n = 5$ (red line), the secondary $n = 6$ (blue line) and the $m = 0$ (black line) modes. The neutron flux in 5(*d*) is plotted in black with a predicted neutron flux (red) from a very simple analysis. The fusion neutron rate

$$\Gamma_n = n_f n_i < \sigma v >_{d-d} \qquad (1)$$

is proportional to fast ion density n_f, the bulk ion density n_i, and the fusion reaction rate $\langle \sigma v \rangle$ which is a strong function of the fast ion energy. The classical slowing time is over 20 ms for these plasma conditions, and is much longer than the measured fast particle confinement times above. Hence, for this simple estimate we assume all ions remain at the injected energy. The density of fast ions within the plasma is a balance between the source and loss rates

$$\frac{\partial n_f}{\partial t} \propto I_{NBI} - \frac{n_f}{\tau_{fi}}. \qquad (2)$$

The red line in figure 5(*d*) uses a single proportionality constant, the measured beam current, and a dynamic fast ion confinement time of $\tau_{fi} = \frac{10\,ms}{\tilde{b}_{n=5}[\%]}$, yielding a 1 ms confinement time at $n = 5$ amplitude of 10%. This assumption matches the asymptotic dependence gleaned from figure 3. Finally in figure 5(*e*) the time dependent energy distribution of fast ions is plotted, measured by a tangential viewing neutral particle analyzer (NPA) [16] which relies on charge exchange with background neutrals to liberate the core-localized, high pitch fast ions [17]. This serves to justify the assumption of fast ions remaining at the injection energy of 25 kV, noting that there is little signal for significantly slowed particles; the lower band of signal corresponds to the half energy component of injected ions. Furthermore, there is a very rapid drop in measured NPA

flux at the onset of QSH; this is due to both a drop in fast ion content and an abrupt change in the magnetic topology (and pitch of the magnetic field lines intersecting the NPA line of sight) at the QSH transition. These data are another clear indicator in the change in fast particle behavior in the QSH RFP state.

Figure 5(*d*) is not a measurement of fast ion confinement; rather it is utilizing the confinement measurements above. It is important to reiterate that the fast ion confinement times are measured at low fast ion concentrations from the beam blip technique. If allowed to reach a high density, energetic ions can excite instabilities that greatly enhance their radial transport [18, 19] and can alter the equilibrium. The latter point is investigated further in the next section.
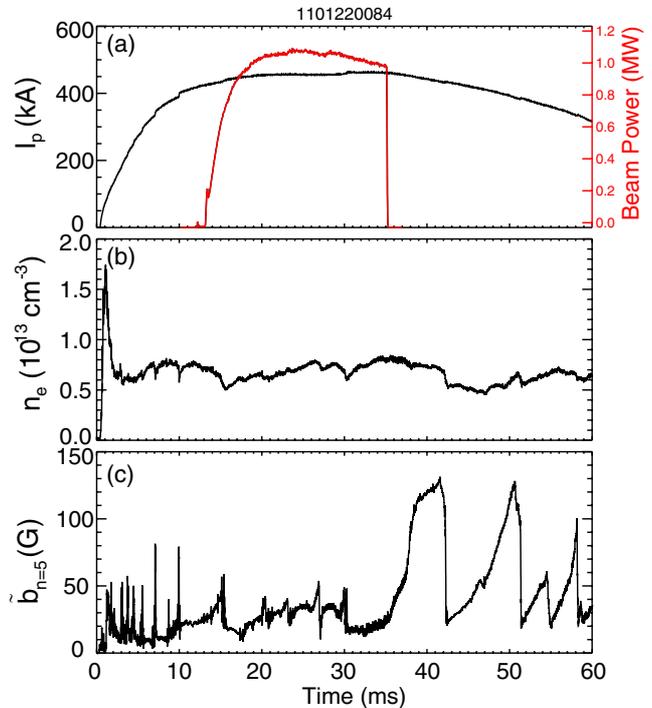
3. Fast ion suppression of QSH transition

The physics of the transitions between axisymmetric and QSH states (in both directions) of the RFP is not fully understood, but the transition into QSH can be encouraged by pushing toward high plasma current at low density and weak edge toroidal magnetic field. Neutral beam injection alters the balance of the competing factors for this transition.

While figure 5 is an example of a transition to QSH during NBI at 500 kA, the likelihood is substantially reduced by NBI. The effect of NBI is most easily seen by targeting plasmas with more marginal transition conditions by lowering the plasma current. Figure 6(*a*) is a typical example of NBI into a 450 kA discharge, with 6(*b*) showing the line-averaged electron density (again at the lower end of the MST operating range). The transition to QSH (or rather, the *first* transition to QSH in this discharge) occurs immediately following beam turn-off. This behavior is quite common, as illustrated in the set of histograms in figure 7.

In figures 7(*a*) and (*b*), a set of 300 kA discharges is investigated for the time of the first transition into QSH with and without NBI. While 300 kA plasma current only makes for marginal transition to QSH (the non-NBI set fails to make the transition at any point in the discharge about 10% of the time) the effect of the beam is obvious. While a substantial number of transitions occur during the 15–35 ms time period without the beam, figure 7(*b*) shows that NBI, which is active during $t = 15$–35 ms, suppresses the transition. In figures 7(*c*) and (*d*), the experiment is repeated at a higher current of 450 kA; here the non-NBI case transitions to QSH 100% of the time in the set of discharges studied, with the first onset occurring with a normal distribution about 22 ms (approximately). The effect of NBI in this higher current case is not to completely suppress the transition, but to delay the onset, with a significant increase in the number of transitions following NBI turn-off.

Without detailed understanding of the mechanism governing transition to QSH, it is provocative to bring up another effect of NBI in the RFP. Further reduction of plasma current and a slightly higher electron density avoids transitions to the QSH state altogether, and a collection of such discharges (many similar discharges, both with and without NBI, are averaged together) is shown in figure 8. The plasma current and NBI power are in figure 8(*a*); in figure 8(*b*) the fusion
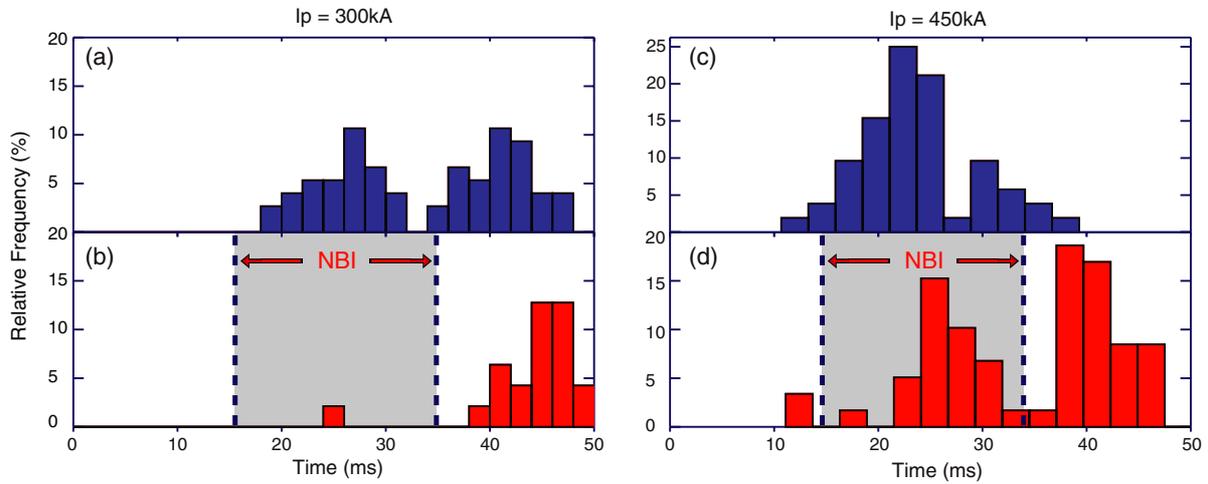

Figure 6. Typical example of delayed QSH onset by NBI. In panel (*a*), the plasma current and NBI power are shown; in (*b*) the line-averaged electron density, and in (*c*) the $n = 5$ mode amplitude is measured. The transition to QSH is indicated by the rapid growth in the $n = 5$ amplitude; in this typical case the transition is delayed until NBI turns off.
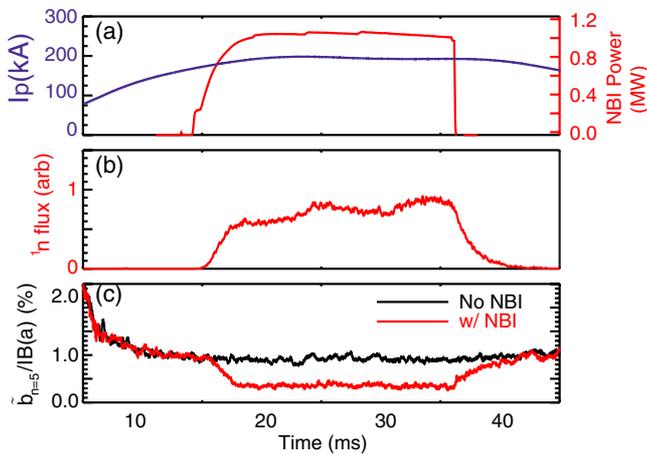
neutron flux for the NBI-injected set of shots is plotted in red (the neutron measurement is zero for the non-NBI cases), and the amplitude of the core-most tearing mode is plotted in figure 8(*c*). The non-NBI discharges (black curve) demonstrate, on average, a very stable value of edge-measured mode amplitude of about 1% of the equilibrium field strength at the edge. With NBI, the mode amplitude is immediately reduced, and continues to get smaller while the neutron flux (rough measure of total fast ion content) increases rapidly. The mode amplitude is nearly constant after about 2 ms of shrinking, and returns to its non-NBI level after beam turn off. The time scales of the decay of neutron flux and mode amplitude suppression match. These data support the argument that rapid growth of the core-most tearing mode, coupled with a decrease in inter-mode energy transfer, can lead to establishment of the QSH state. However, this problem remains a very interesting and relevant open topic.

4. Discussion

The MH to QSH transition remains a unique problem to the RFP, but the confinement of fast ions in a 3D field is a topic with connections to other magnetic configurations. There is a well-established knowledge base for transport in stellarators, and, historically, a primary deficiency of stellarators has been elevated transport due to non-axisymmetry [20]. The recent results of energetic ion transport in the RFP, which avoids the stochasticity-induced Rechester-Rosenbluth-like transport [21], may present a new region in parameter space for

Figure 7. Histograms of the onset of QSH for varying plasma conditions with and without NBI. In (*a*) and (*b*), the QSH onset time in 300 kA plasmas with and without NBI is plotted. The no NBI case is marginally conducive to a QSH transition, with about 90% of the discharges transitioning; in (*b*) the transitions are delayed until after NBI. In the 450 kA case shown in (*c*) and (*d*), the QSH transition without NBI occurs reliably with a normal distribution about $t = 22$ ms; with NBI the distribution of QSH onset is significantly delayed.

Figure 8. NBI affects the core-most tearing amplitude; the effect is most apparent at lower plasma current where there is no transition to QSH. Several discharges, both with and without NBI, are averaged together. Plotted in panel (*a*) is the average plasma current for all discharges along with the NB power for the beam on subset; in panel (*b*) the d–d fusion neutron flux for the beam-on case is plotted in red (the fusion neutron flux for the no-beam case is zero); panel (*c*) plots the $n = 5$ mode amplitude for the no-beam case in black and the NB-injected case in red. There is a substantial drop in mode amplitude coinciding with NB turn on; a lower mode amplitude is sustained until the beam is turned off, and the amplitude returns to the level of the no-beam case on the same timescale as the neutron flux decay.

study of the non-axisymmetry related transport. Generally, neoclassical effects are ignored in the RFP. It is a newly opened topic, indeed, but investigation of the the $1/\nu$ 'superbanana' branch of transport may be important in the RFP, as finite amplitudes of secondary magnetic perturbations may lead to an analogous ripple trapping of fast ions. Furthermore, with the lower collisionality of fast ions, enhanced banana drift may be a significant contributor to the measured radial transport. This mechanism is also driven by the non-axisymmetry factor ϵ_h; its importance relative to other neoclassical transport effects is yet to be studied in the RFP. Orbit modeling of the energetic ions

in the 3D QSH-like RFP equilibrium is thus a fascinating and important topic for immediate consideration; this technique has recently been employed for thermal particles in the 3D state of the RFX-mod device [22].

5. Summary

Fast ions are well confined in the axisymmetric RFP with modestly stochastic magnetic field. As such, a high concentration of fast ions develops during neutral beam injection and has several effects on the RFP plasma. These include the expected heating and momentum injection, the excitement of energetic ion driven modes, and a reduction of core-most tearing mode amplitude. The presence of fast ions from NBI delays the transition to the QSH state, perhaps indicating a link between core-most tearing mode and the onset of QSH. Once established, the QSH state presents a plasma where fast ion confinement is reduced from the classical levels, but is larger than that expected for stochastic transport (where radial transport is proportional to parallel speed). To date, no interesting energetic ion driven phenomena have been observed in the QSH RFP, likely because the reduction in confinement leads to a smaller fast ion density.

References

[1] Heidbrink W W and Sadler G J 1994 *Nucl. Fusion* **34** 535–615
[2] Mynick H E 1993 *Phys. Fluids* B **5** 1471–81
[3] Akers R J *et al* 2002 *Nucl. Fusion* **42** 122–35
[4] Fiksel G, Hudson B, Hartog D J D, Magee R M, O'Connell R, Prager S C, Beklemishev A D, Davydenko V I, Ivanov A A and Tsidulko Y A 2005 *Phys. Rev. Lett.* **95** 125001
[5] Liu D *et al* 2011 *Proc. 5th IAEA Energetic Particle Meeting (Austin, TX)*
[6] Lorenzini R *et al* 2009 *Nature Phys.* **5** 570–4
[7] Bergerson W F *et al* 2011 *Phys. Rev. Lett.* **107** 255001
[8] Martin P *et al* 2000 *Phys. Plasmas* **7** 1984
[9] Heidbrink W W, Kim J and Groebner R J 1988 *Nucl. Fusion* **28** 1897–901

[10] Chapman B E *et al* 2012 *Proc. 24th IAEA Fusion Energy Conf. (San Diego, CA)*

[11] Anderson J K *et al* 2013 *Phys. Plasmas* **20** 056102

[12] Dexter R N, Kerst D W, Lovell T W, Prager S C and Sprott J C 1991 *Fusion Technol.* **19** 131–9

[13] Prager S C *et al* 1995 *Plasma Phys. Control. Fusion* **37** A303

[14] Reusch J A, Anderson J K and Tsidulko Y A 2014 *Nucl. Fusion* **54** at press

[15] Reusch J A, Anderson J K, Hartog D J D, Ebrahimi F, Schnack D D, Stephens H D and Forest C B 2011 *Phys. Rev. Lett.* **107** 155002

[16] Polosatkin S *et al* 2011 *Fusion Sci. Technol.* **59** 259–61

[17] Eilerman S, Anderson J K, Reusch J A, Liu D and Fiksel G 2012 *Rev. Sci. Instrum.* **83** 10D302

[18] Koliner J J *et al* 2012 *Phys. Rev. Lett.* **109** 115003

[19] Lin L *et al* 2013 *Phys. Plasmas* **20** 030701

[20] Mynick H 2006 *Phys. Plasmas* **13** 058102

[21] Rechester A B and Rosenbluth M N 1978 *Phys. Rev. Lett.* **40** 38–41

[22] Gobbin M, Spizzon G, Marrelli L and White R B 2010 *Phys. Rev. Lett.* **105** 195996